American Mineralogist, Volume 82, pages 99–108, 1997

# Memory effects of domain structures during displacive phase transitions: A high-temperature TEM study of quartz and anorthite

HONGWU XU AND PETER J. HEANEY

Department of Geosciences and Princeton Materials Institute, Princeton University, Princeton, New Jersey 08544, U.S.A.

## ABSTRACT

Memory effects associated with the Dauphiné twins in α quartz and the c-antiphase domains (c-APDs) in $P\bar{1}$ anorthite have been investigated by in situ hot-stage transmission electron microscopy (TEM). In a set of kinetic experiments, specimens were cycled about their transition temperatures, and changes in the Dauphiné twin and c-APD positions were analyzed as a function of maximum annealing temperature and annealing time. The results indicate that Dauphiné twins are strongly pinned by extended defects, such as Brazil twin and grain boundaries, dislocations, and surfaces. However, the memory displayed by Dauphiné twin boundaries pinned by point defects degrades with higher annealing temperatures and longer annealing times. An Arrhenius analysis of this behavior yielded an average activation energy for point-defect diffusion of 68.6 kJ/mol.

In contrast to the Dauphiné twins of quartz, the c-APDs of anorthite did not appear to interact strongly with extended defects, and they exhibited a nearly perfect memory for all annealing times and temperatures tested. This extremely high fidelity is interpreted as evidence that the positions of c-APDs are fixed by localized Al-Si disorder, which remains unchanged when anorthite is heat treated at <1000 °C.

## INTRODUCTION

Memory effects involving the mechanical, optical, and electrical properties of materials are of importance for both theoretical and practical reasons (Jamet 1988; Strukov 1989; Liu et al. 1992; Warren et al. 1996). For instance, when a shape-memory alloy is deformed under stress, it recovers its original morphology upon heating above a critical temperature. Underlying this phenomenon is a martensitic transformation that creates a twinned phase during the down-temperature transformation (Perkins 1981). Deformation of the low-temperature martensitic phase is associated with unusually low elastic strain because the twinned low-temperature structure can accommodate slip through a variety of mechanisms that are controlled by the twin-composition planes. When the alloy is heated above its critical point, the martensite lamellae disappear and the original shape is restored, allowing application of such alloys in heat-sensitive electronic switches and orthodontic devices (Wayman 1980; Liu et al. 1992).

In some alloy systems, the materials display a "two-way shape memory" (Wayman 1980). After deformed specimens have been heated above the transition temperature to regenerate the initial morphology, the alloys can recover the deformed morphology upon recooling to the martensitic state. Such materials can be induced to deform and recover repeatedly by cycling the material about the transition temperature in a process known as "microstructural training."

Several natural materials exhibit memory effects similar to the two-way memory observed among certain alloys. Although shape recovery has not been reported for minerals (and seems unlikely in light of their brittle behavior), strong microstructural memory has been recognized for more than one-half century. In minerals such as leucite (Wyart 1938; Peacor 1968; Sadanaga and Ozawa 1968; Mazzi et al 1976; Heaney and Veblen 1990), manganoan pigeonite (Gordon et al. 1981; Carpenter 1994), quartz (Frondel 1945; Young 1962; Inoue et al. 1974; Zarka 1983; Malov and Sonyushkin 1976; Dolino and Bachheimer 1982; Heaney and Veblen 1991), and anorthite (Müller and Wenk 1973; Heuer et al. 1976; Ghose et al. 1988; Smith and Brown 1988; Van Tendeloo et al. 1989), these memory phenomena follow similar patterns: When the low-temperature phase is heated above a displacive transition temperature, $T_c$, and then cooled below it, the twins or antiphase domains that populated the original low-temperature phase reappear in the same positions and orientations.

Of course, such memory effects are not surprising when they characterize domains that never truly disappear above $T_c$. For instance, transmission electron microscope (TEM) observation of the pseudomerohedral twins of leucite has revealed their existence well above $T_c$ (Heaney and Veblen 1990). However, the recovery of Dauphiné twins in quartz and of c-antiphase domains (c-APDs) in anorthite is more problematic. Hot-stage TEM studies of both minerals have unambiguously demonstrated the disappearance of these domains through boundary-wall migration and microtwinning at their phase transitions

0003–004X/97/0102–0099$05.00

(Müller and Wenk 1973; Van Tendeloo et al. 1976). In such minerals, the retention of domain information during temperature cycling is not explicable on a purely crystallographic basis because the symmetry operations that underlie the twin laws are fully restored above $T_c$. Some researchers have suggested that point defects pin the domain boundaries within quartz (e.g., Heaney and Veblen 1991) and anorthite (Van Tendeloo et al. 1989), whereas others believe that the memory effect may result from internal strains (Zarka 1983).

In this study, we explored memory mechanisms in minerals by measuring the dependence of memory loss on annealing times and temperatures. Several sets of kinetic experiments were performed by in situ heating of specimens within the TEM accompanied by systematic variation of heating periods and maximum temperatures. Degradation of domain memory was quantified following the procedure used in Heaney and Veblen (1991), and for the first time an Arrhenius analysis of the memory loss was applied to ascertain activation energies associated with defect diffusion. Differences in the memory behavior exhibited by quartz and anorthite suggest subtle differences in the causes of domain retention.

## Crystallographic background

### The α-β quartz transition

The transition from β to α quartz results from a distortion of the tetrahedral chains that transforms the β structure from hexagonal to trigonal (reviewed in Heaney 1994). The distortion is effected by the tilting of tetrahedra in one of two possible orientations, which results in two distinct Dauphiné twins. These twins are related by the twofold rotation parallel to the $c$ axis that is contained within the sixfold screw axis of β quartz ($P6_422$ or $P6_222$) but absent in α quartz ($P3_121$ or $P3_221$).

The Dauphiné domains can be imaged by dark-field TEM methods using appropriate diffractions, such as 301. Van Tendeloo et al. (1976) and Malov and Sonyushkin (1976) observed that large Dauphiné domains disperse into microtwins over a temperature interval of 1.3 °C between α and β quartz. Later theoretical and experimental results (e.g., Aslanyan et al. 1983; Bachheimer 1980) demonstrated that these microtwins constitute a stable incommensurate intermediate phase. Therefore, the α-β quartz transformation is divided into an α quartz–IP (intermediate phase) transition at $T_c$ = 573 °C and an IP-β quartz transition at $T_i$ = 574.3 °C. The first transition appears to be first order, whereas the subsequent transition probably is second order.

### The $P\bar{1}$-$I\bar{1}$ transition in anorthite

The $P\bar{1}$-$I\bar{1}$ anorthite transition was first discovered by Brown et al. (1963) with high-temperature single-crystal X-ray diffraction, and subsequent studies using various techniques have placed $T_c$ at ~241 °C for pure metamorphic anorthite samples (e.g., Laves et al. 1970; Staehli and Brinkmann 1974; Adlhart et al. 1980; Ghose et al. 1993). The down-temperature inversion of $I\bar{1}$ to $P\bar{1}$ anorthite involves a change from body-centered to primitive symmetry while conserving unit-cell size. As reviewed by Nord (1992), such a transition produces c-APDs that are related by the lost translation vector ½[111]. The c-antiphase domain boundaries (c-APBs) can be imaged by dark-field TEM with either the c ($h + k$ = even; $l$ = odd) or d ($h + k$ = odd; $l$ = even) reflections, but because the c reflections are more intense, they provide superior contrast. Anorthite also experiences an Al-Si ordering transformation that involves a symmetry change from $C\bar{1}$ to $I\bar{1}$ at ~2039 °C, which is above the melting point (Heuer and Nord 1976; Carpenter 1988).

Previous studies by X-ray, neutron, and electron diffraction techniques (Laves et al. 1970; Czank et al. 1973; Foit and Peacor 1973; Adlhart et al. 1980; Van Tendeloo et al. 1989) have revealed that the c reflections, which violate $I\bar{1}$ symmetry, do not entirely disappear when $T > T_c$. Although both diffraction studies and NMR measurements (Staehli and Brinkmann 1974; Phillips and Kirkpatrick 1995) suggest that a body-centered Al-Si framework is achieved above $T_c$, structural refinements also indicate that the Ca atoms occupy split positions, mimicking their distribution in the primitive structure (Megaw et al. 1962; Czank et al. 1973; Smith 1974; Van Tendeloo et al. 1989; Ghose et al. 1993). Some of these researchers (Ghose et al. 1988; Van Tendeloo et al. 1989; Ghose et al. 1993) concluded that the $I\bar{1}$ structure actually is a statistical average of c-antiphase microdomains that fluctuate in response to a dynamical oscillation of Ca atoms between two sets of $P\bar{1}$ positions within an $I\bar{1}$ aluminosilicate framework. The nature of the $P\bar{1}$-$I\bar{1}$ phase transition largely depends on the degree of Al-Si order and the amount of substitution of Na for Ca in anorthite: Tricritical behavior is observed for end-member anorthite with complete Al-Si order, whereas Al-Si disorder and Na impurities impart a second-order character to the transition (Salje 1987; Redfern and Salje 1987; Redfern et al. 1988; Redfern and Salje 1992; Redfern 1992). In addition, Al-Si disorder appears to decrease $T_c$, whereas an albitic component increases it (Redfern 1992).

## Experimental methods

The quartz and anorthite samples employed in this study were kindly supplied by the U.S. National Museum (quartz: USNM no. R17684-2; anorthite: USNM no. B19995). The quartz sample is a transparent, doubly terminated crystal from Hot Springs, Arkansas. The anorthite specimen is a reddish, ~1 cm crystal from Toal della, Val di Fassa, Monzoni, Italy (Table 1). Thin sections were cut normal to the morphologic $c$ axis of quartz and parallel to (001) of anorthite and thinned further by Ar-ion milling. Unsupported foils of 3 mm diameter were then coated lightly with amorphous carbon.

Electron microscopy was performed in the General Motors Electron Beam Facility of the Princeton Materials Institute. Quartz was examined with a Philips 400 microscope equipped with a standard twin objective lens and operated at 100 keV. TEM observations of anorthite were

**TABLE 1.** Chemical compositions (wt%) of anorthite

| | |
|---|---|
| $SiO_2$ | 42.80 |
| $Al_2O_3$ | 37.98 |
| $Fe_2O_3$ | 0.04 |
| CaO | 20.65 |
| $Na_2O$ | 0.01 |
| Total | 101.48 |

*Note:* Anorthite sample was analyzed with a Cameca SX-50 electron microprobe operated at 15 kV and 15 nA. Formula: $(Ca_{1.008}Na_{0.001})(Si_{1.950}Al_{2.040}Fe_{0.001})O_8$.

conducted using a Philips CM-20 microscope equipped with a supertwin objective lens and operated at 200 keV. Heating experiments were performed with a Gatan model 652 double-tilt heating holder. Specimens were heated by an annular tantalum furnace, which warmed in response to an increase in electrical current through a molybdenum strip heater. Furnace temperatures were registered by a Pt-13% Rh thermocouple spot welded to the furnace body. The difference in temperatures between the furnace and the thin edge ranged from 15 to 95 °C because of poor thermal conductivity. Nevertheless, the furnace temperature corresponding to the critical temperatures of the specimens could be inferred from the abrupt changes in the configuration of the Dauphiné twins and c-APDs.

Kinetic experiments were performed by heating an individual specimen at a maximum temperature $>T_c$ for a specified annealing time and quenching the specimen below $T_c$ by rapidly decreasing electrical current to the furnace. As specified below, individual samples were cycled in this fashion about $T_c$ with variations in either the maximum temperature or the annealing time. The temperature of overheating ($\Delta T_o$) is defined as the difference between the maximum annealing temperature, $T_{max}$, and the transition temperature, $T_c$ (i.e., $\Delta T_o \equiv T_{max} - T_c$).

For quartz, seven separate experiments were conducted using seven foils. Values for $\Delta T_o$ included 2, 5, 10, 20, 50, and 100 °C (for 2 experiments), and the annealing time at $T_{max}$ was increased from cycle to cycle in the following sequence: 1, 10, 20, 50, 100, 200, 500, 1000, and 2000 s. Experiments with anorthite were conducted under the following conditions: (1) $\Delta T_o$ was held constant at 350 °C, and annealing time at $T_{max}$ was increased from 1 to 2000 s; (2) $\Delta T_o$ was increased in successive cycles from 100 to 700 °C with an interval of 100 °C, and annealing time at $T_{max}$ was held constant at 600 s.

Dark-field TEM photographs of a given twin configuration were scanned using an Apple scanner with a resolution of 300 dpi. Memory loss was measured by superimposing the scanned image of one domain configuration on that associated with the preceding cycle using Adobe Photoshop 3.0. The areas of the mismatched regions were digitized and integrated by an in-house graphics program. Following the method adopted by Heaney and Veblen (1991), the percentage of memory loss ($M$) was calculated by dividing the sum of the areas of mismatch by the total area examined. Thus, $M$ represents the change in twin configuration from one cycle to the next, rather than the cumulative change from the first to the final configuration.

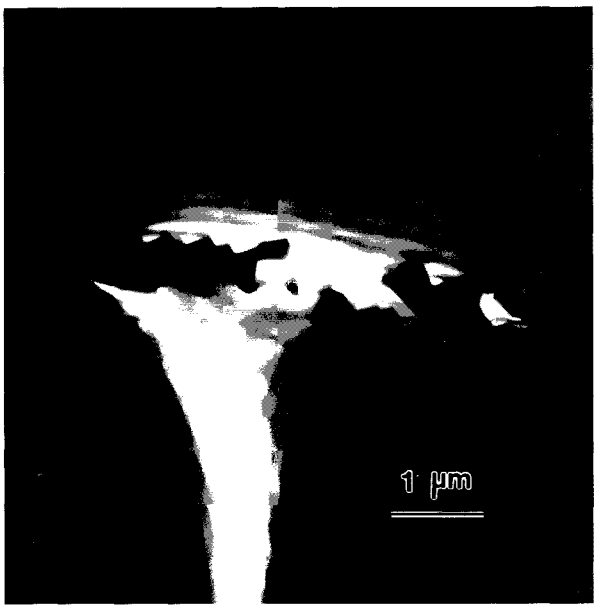


**FIGURE 1.** Dark-field image of Dauphiné twins. The twins are pinned by the grain boundaries.

## RESULTS AND ANALYSIS

### Memory behavior in quartz

**Interactions of twins and extended defects.** Frondel (1945) and Zarka (1983) demonstrated a close spatial association between Dauphiné twins and fractures. Likewise, before our heating experiments, the quartz specimens contained virtually no Dauphiné twin boundaries, but after cycling specimens about $T_c$, the Dauphiné domain walls commonly appeared near grain (Fig. 1) and Brazil twin boundaries (Fig. 2). As also described by Van Goethem et al. (1977), the Dauphiné twin walls did not transect the Brazil twin boundaries, and when the temperature was increased above $T_c$, the microtwin mosaics remained encaged within the static Brazil twin domains (Fig. 2A), with no apparent interaction among individual sets of microtwins in adjacent domains.

Similarly, surface strain dictated the configuration of Dauphiné twins near the thin edges of the specimen foils. As seen in Figure 3, small Dauphiné twins frequently speckled the foils near edges and holes, and these tiny twins typically did not grow with decreasing temperature. As indicated by diffraction contours in TEM images, the strain associated with these edges is quite pronounced and idiosyncratic, as the ratio of surface to volume tends toward infinity and the foil begins to bend under its own weight.

The tendency of Dauphiné twin walls to cluster near such extended defects as dislocations, grain boundaries, and edges may be attributed to the strain fields localized around them. The heightened strain potential near these

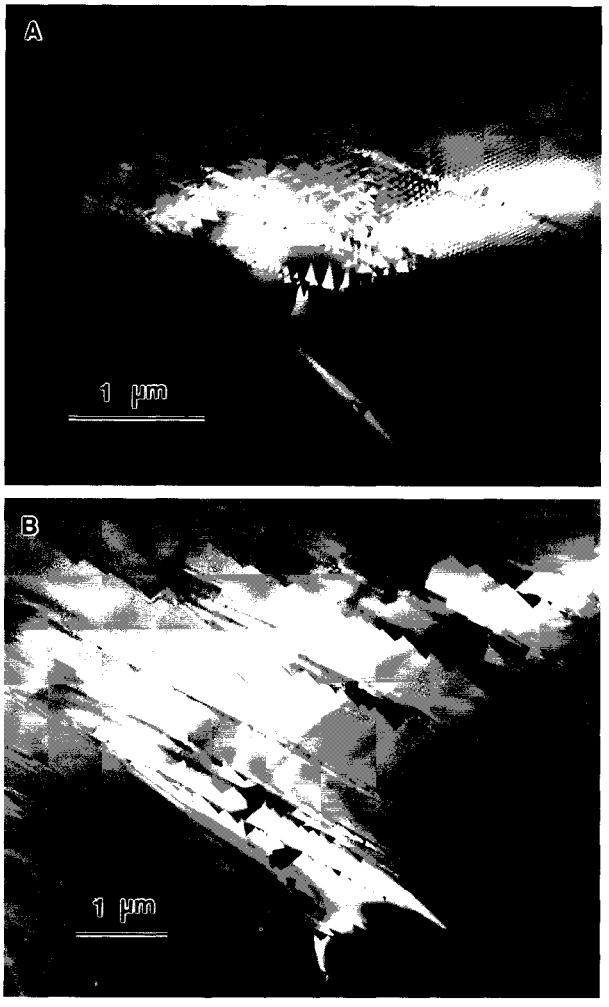


FIGURE 2. Configurations of Dauphiné microtwins (**A**) and macrodomains (**B**) are controlled by Brazil twin boundaries.

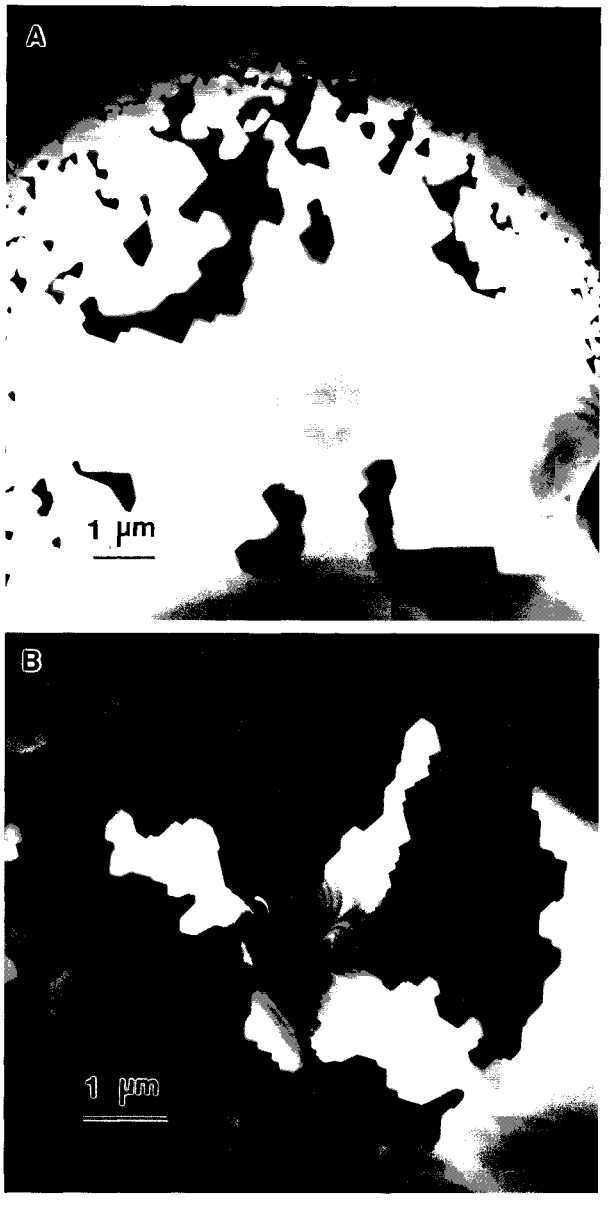


FIGURE 3. Dark-field images of Dauphiné twins. Twins are pinned by surface strain (**A**) along the thin edge of the specimen at the top of the image and (**B**) around a hole within the foil.

features lowers the energy difference between the host crystal and the Dauphiné twin walls, which themselves are centers of structural strain. As the twin boundaries per se are structurally similar to β quartz (the order parameter within the wall is 0) (Liebau and Böhm 1982; Walker 1983), these strain fields effectively stabilize the β quartz structure and renormalize the transition temperature downward. This interpretation is supported by differential thermal analysis of fine-grained defective quartz samples (Sosman 1965), in which the α-β quartz transition broadens over temperatures <573 °C. In addition, in their TEM study of deformed quartzite, Barber and Wenk (1991) noted that patches of microtwinned intermediate phase persist in areas of high dislocation densities when the bulk crystal is well below the nominal transition temperature.

The strain fields produced by extended defects significantly constrain the net movement of Dauphiné twin boundaries. To quantify this effect, we cycled quartz specimens about $T_c$ and measured the degree of memory loss near a subgrain boundary and near a thin foil edge. Figure 4A reveals the dependence of memory loss on the annealing time above $T_c$ with overheating by 2 and 100 °C for the thin edge and the subgrain boundary, respectively. Although some variation in twin positions is reflected in these measurements, the degree of fidelity is remarkably high, with memory loss rarely exceeding 2%. In one experiment, the twin configuration adjacent to the subgrain boundary achieved 99% retention even after heating 100 °C above $T_c$ for 2000 s (≈33.3 min). These results suggest that Dauphiné twins are essentially immobilized in highly defective quartz. To the extent that

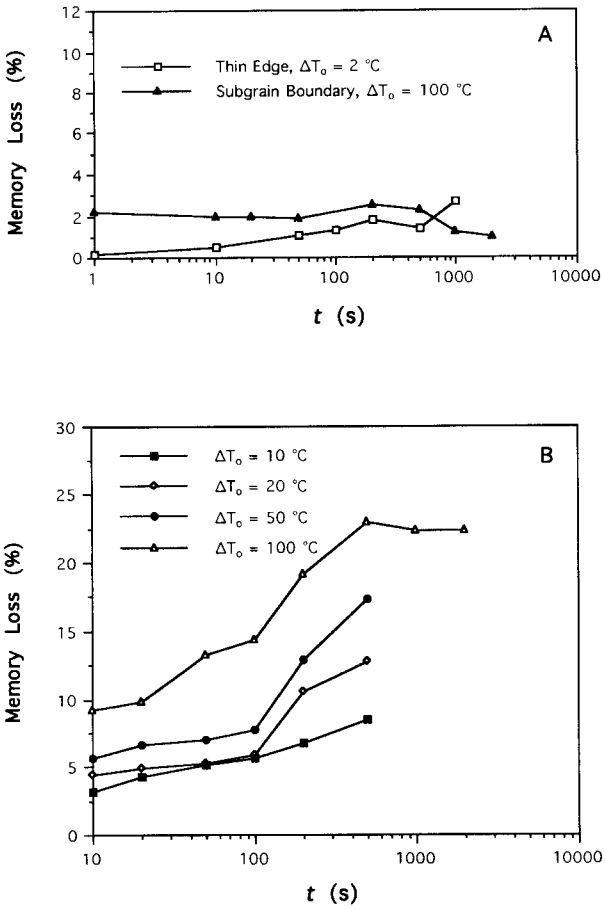


**FIGURE 4.** Dependence of memory loss on annealing time, with temperature of overheating, $\Delta T_o$, constant. Data points represent memory loss per cycle. (**A**) Memory loss for twins adjacent to extended defects, such as a thin edge ($\Delta T_o$ = 2 °C) and a subgrain boundary ($\Delta T_o$ = 100 °C). (**B**) Memory loss for twins not in the neighborhood of visible defects.

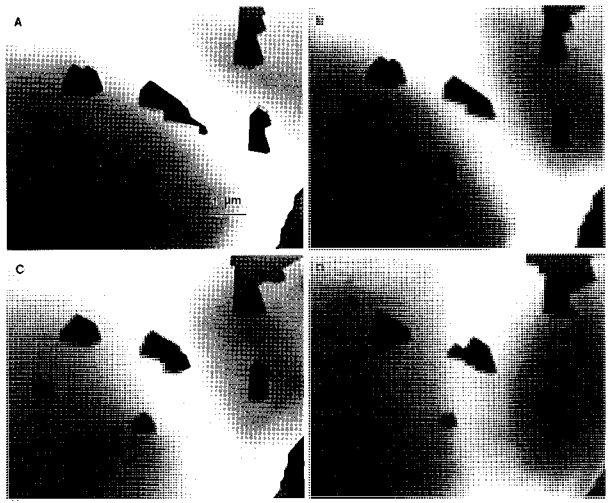


**FIGURE 5.** Selected dark-field images of Dauphiné twins after the specimen was cycled repeatedly about $T_c$, with $\Delta T_o$ = 5 °C. (**A**) Original configuration, (**B**) annealing time at $T_{max}$ = 10 s, (**C**) 50 s, (**D**) 200 s.

these twin boundaries can accommodate strain (Frondel 1945) and prevent dislocation creep, inhibition of twin-boundary movement might lead to increased brittleness in deformed quartz crystals.

**Pinning by point defects.** Strain fields resulting from extended structural defects that are visible by transmission electron microscopy cannot be the only cause of memory behavior in quartz. The Hot Springs, Arkansas, specimen used in the present study contained virtually no inclusions, and subgrain boundaries, dislocations, and Brazil twin walls occurred in extremely low densities ($\ll 10^8$ cm$^{-2}$). Nevertheless, Dauphiné twins displayed strong memory effects even in regions with no discernible imperfections. The degree of twin-boundary retention in defect-free areas, however, was noticeably lower than in highly defective zones.

In a previous study, Heaney and Veblen (1991) quantitatively measured memory loss after they had cycled defect-free specimens about the transition, and they ascribed this memory behavior to the influence of point defects. Small shifts in boundary positions were attributed to the diffusion of these defects. Natural quartz crystals commonly contain point defects in concentrations of hundreds of parts per million (Frondel 1962), and they can occur in the form of vacancies, interstitials, and substitutions (O'Brien 1955; Cohen 1985; Freer 1981). Just as the APBs in pigeonite can accommodate large cations such as $Ca^{2+}$ (Morimoto and Tokonami 1969; Carpenter 1978; Gordon et al. 1981; Carpenter 1994), the more open β quartz–like framework associated with the Dauphiné twin boundaries should serve as energetically favorable sites for interstitial cations.

To confirm this interpretation and to extract activation energies for defect migration, we performed a systematic series of heating experiments with variations in both annealing time and temperature of overheating for regions that were free of extended defects. Figure 5 reveals the changes in twin-boundary configuration from one cycle to the next in a typical experiment, and overall measurements of memory loss are presented in Figure 4B. As indicated by these results, the degree of memory loss consistently increased with longer annealing times and with higher annealing temperatures. Because defect diffusion is a thermally activated process, these results are consistent with a mechanism in which point defects control the positions of the twin boundaries.

High-quality measurements of memory loss in a temperature-time series allow the determination of activation energies associated with point-defect diffusion. The rationale for this approach is based on the assumption that memory loss is a linear function of the diffusion coefficient, i.e., memory loss ($M$) = a × diffusion coefficient ($D$), where a is a constant. The diffusion coefficient, $D$, typically follows an Arrhenius relation and can be ex-

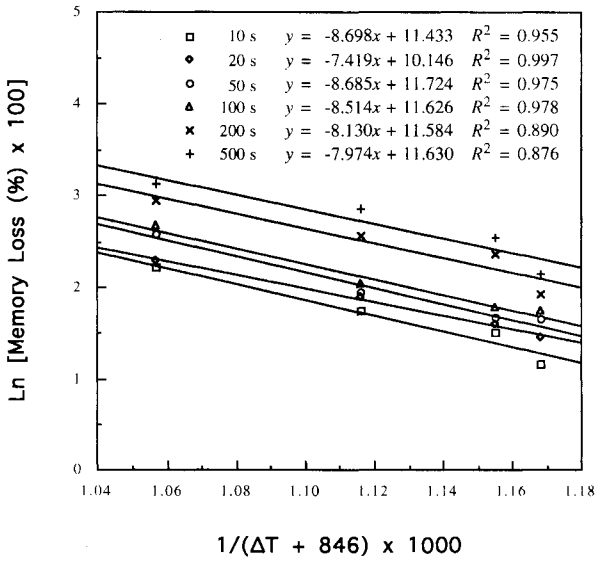


**FIGURE 6.** The dependence of the natural log of the memory loss on $1/T$ for twins constrained by no visible defects. Twin configurations for different annealing times reveal linear Arrhenius behavior with similar slopes and intercepts.

pressed in the form $\ln D = \ln D_0 - Q/RT$, where $D_0$ is the diffusion constant at infinite temperature ($1/T = 0$), $Q$ is the activation energy, and R is the universal gas constant (see Manning 1968, for review). If the assumption that $M = aD$ holds, then the memory loss also should obey an Arrhenius function: $\ln M = \ln M_0 - Q/RT$. In other words, the dependence of $\ln M$ on $1/T_{max}$ should be linear for those experiments in which the annealing time was held constant.

With some degree of scatter, our experimental results do support this inference over our temperature range of 847.5–947.5 K (Fig. 6). Correlation factors for linear fits ranged from 0.876 to 0.997, and the slopes and intercepts for the six annealing times are remarkably similar. In theory, these values should be identical. The slopes of these lines yield an average activation energy of 68.6 kJ/mol, which is well within the range of activation energies as determined by more conventional methods (Table 2). Our measured value for this activation energy suggests that the mechanism responsible for the memory effect does not involve the breaking of Si-O bonds, which would require energies on the order of 227.675 kJ/mol (Robie et al. 1978). Rather, on the basis of the diffusion experiments listed in Table 2, it seems likely that the defects consist of interstitial species within the tunnels parallel to the $c$ axis. It is impossible to image individual point defects during heating experiments because of insufficient instrumental resolution and specimen drift, and we could not identify the diffusing species within the specimens. Thus, the activation energy obtained represents an overall value for point-defect diffusion. In addition, we cannot determine the value of the preexponential factor $D_0$ because the coefficient a remains unknown.

**TABLE 2.** Activation energy values for point-defect diffusion in quartz

| Diffusing species | $Q$ (kJ/mol) | $T$ range (K) | Method* |
|---|---|---|---|
| $^{45}Ca$ | 284.0 | 873–1073 | // $c$, RA |
| Na | 102.4 | 673–1273 | TE |
| $^{22}Na$ | 113.0 | 873–1063 | $\perp$ $c$, RA |
| $^{22}Na$ | 48.0 | 873–1073 | // $c$, RA |
| $D^+$-$H^+$ | 79.4 | 673–873 | // $c$, IR |
| — | 68.6 | 847.5–947.5 | This study |

* All values from Freer (1981) except for those from this study. RA = residual activity analysis; TE = tracer experiment; IR = infrared analysis, exchange with $D_2O$.

A few sources of experimental error may lessen the accuracy of the above analysis: (1) In the course of our runs, we made an effort to cool and heat samples instantaneously and to keep the minimum holding temperature constant, but deviations from this ideal become more significant with shorter annealing times and higher temperatures of overheating. (2) Although $T_c$ may be pinpointed exactly by the appearance of the intermediate phase, gauging the temperature of overheating is complicated by the temperature gradient between the furnace and the specimen. Our measurements assumed that this temperature gradient is a linear function of distance from the furnace. (3) Because point-defect diffusion can occur at temperatures $<T_c$, the measured amount of memory loss may be slightly larger than was contributed by annealing at $T_{max}$. (4) It is difficult to confirm that defect-free areas lie completely outside the influence of strain fields associated with extended defects, such as dislocations or specimen edges.

Nevertheless, the correspondence between the activation energies calculated in this study using memory loss and the activation energies of defect diffusion in quartz as determined by other techniques is surprisingly close. This agreement suggests that the errors associated with this method are not overwhelming (unless they fortuitously cancel). In fact, it may be noted that all techniques used to measure diffusion coefficients suffer from systematic errors, and discrepancies in the published diffusion data for a given mineral can be considerable (Freer 1981). Although kinetic analyses of memory loss are prone to experimental difficulties, they offer some promise for measuring diffusion characteristics of materials that undergo phase transitions that are similar to that observed in quartz.

### Antiphase domain behavior in anorthite

**Interaction of APBs with extended defects.** Unlike Dauphiné twins, c-APBs were not observed to concentrate near dislocations and grain boundaries (Fig. 7). Although such extended defects disrupted the continuity of c-APBs, no evidence was discerned for an interaction between the c-APBs and the strains generated by the defects. The absence of such a dependence may be related to the fact that the Dauphiné twin walls are strongly con-


FIGURE 7. Dark-field image of c-APBs and an albite-rich exsolution lamella.

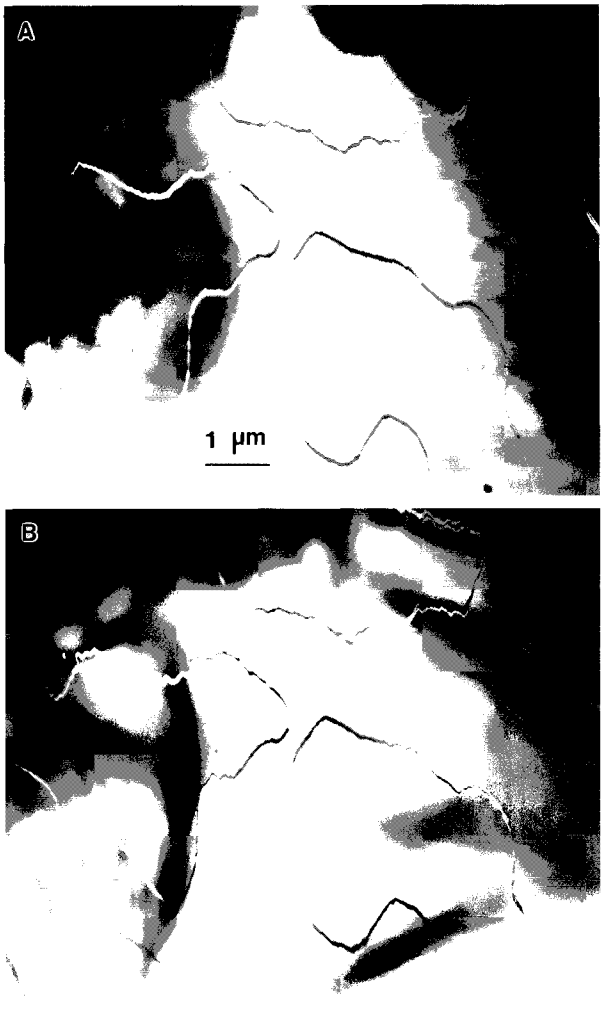


FIGURE 8. Dark-field images of c-APBs. (**A**) Original configuration; (**B**) after the specimen was cycled successively about $T_c$, with $\Delta T_o$ = 350 °C for 1, 10, 20, 50, 100, 200, 500, 1000, and 2000 s.

trolled by strain. Strain-energy minimization requires that Dauphiné boundaries adopt a limited number of orientations, thereby producing a polygonized Dauphiné twin network (Walker 1983). The c-APBs of anorthite, in contrast, freely assume any shape and are not strongly constrained to assume crystallographically controlled positions, although they have a weak tendency to align along the $(2\bar{3}\bar{1})$ plane (Ribbe and Colville 1968; Smith and Brown 1988).

**Memory effects.** In 1973, Müller and Wenk annealed natural anorthite samples over a range of temperatures, and their dark-field TEM images revealed no change in the size distribution and diffraction contrast of c-APDs for samples heated at 500 and 600 °C. However, c domains could not be observed in samples heated at 1200 and 1430 °C. Using an even broader range of annealing temperatures and times, John and Müller (1988) found that the average size of c-APDs remained unchanged at temperatures up to 1000 °C, but domain size decreased in samples heated to 1200 °C and higher temperatures (see also Müller 1988).

Our examination of anorthite specimens revealed more than a retention of average domain size. When anorthite specimens were subjected to a regimen of heating experiments similar to those conducted for quartz, no change in domain size or shape was discerned during the experiments (Figs. 8 and 9). Even specimens heated for 33 min at 941 °C (such that $\Delta T_o$ = 700 °C) revealed no APB movement within experimental error upon quenching.

Some authors have attributed the memory displayed by anorthite to point defects, particularly Na, but our kinetic analysis suggests that Na is not the factor that controls the memory mechanism. As with virtually all natural samples, the anorthite crystal used in our experiments contained a small amount of $Na^+$ substituting for $Ca^{2+}$ (Table 1). However, by analogy with quartz, if Na impurities pin the c-APBs, then those antiphase boundaries should migrate as a function of temperature because of point-defect diffusion. Although there is no published determination of tracer or self-diffusion coefficients for Na in anorthite or even anorthite-rich plagioclase feldspars (Freer 1981; Brady 1995), several scientists have studied diffusion in alkali feldspars (Table 3).

If the diffusion coefficient for Na in anorthite is of the same order as that in alkali feldspars, then the expected diffusion distance for Na during our experiments should have led to a detectable boundary migration. Depending on the annealing temperature and the reported coefficient, diffusion distances calculated using $x^2 = Dt$, where $x$ is the diffusion distance, range from ~0.5 to 5.0 μm (Table 4). Boundary movement on this scale is easily measured by TEM methods. Thus, in light of the perfect fidelity of the c-APB memory in anorthite, it seems unlikely that pinning by substitutional Na alone is the mechanism for the memory effect.

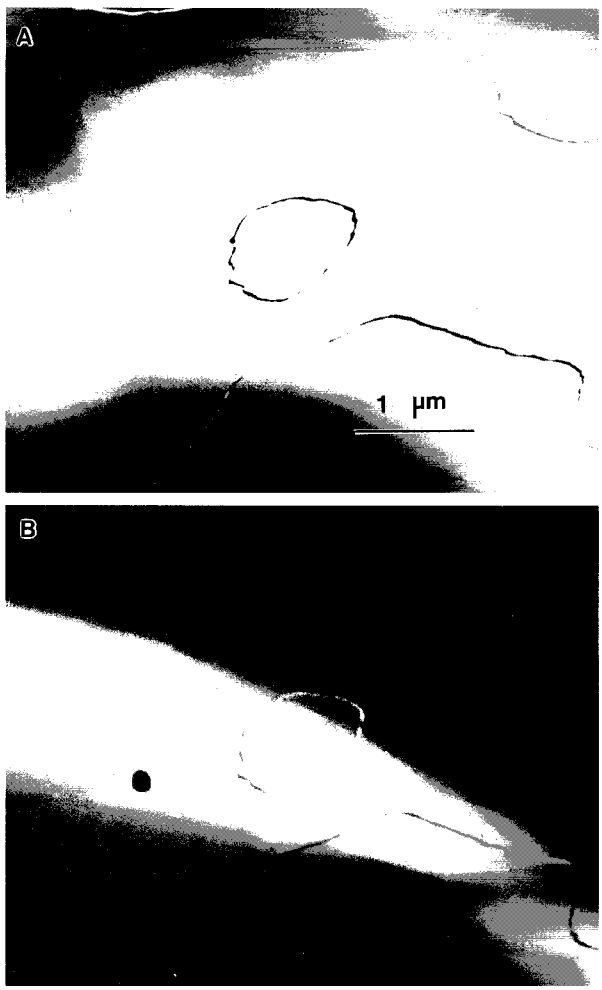


FIGURE 9. Dark-field images of c-APBs. (**A**) Original configuration; (**B**) after the specimen was cycled successively about $T_c$ for 10 min, with $\Delta T_c$ = 100, 200, 300, 400, 500, 600, and 700 °C.

**Effect of Al-Si order.** The Al-Si distribution in slowly cooled anorthite is completely ordered. Within the fourfold and eightfold rings of the framework, $SiO_4$ and $AlO_4$ tetrahedra alternate so that each bridging O atom is bonded to one Si atom and one Al atom (Si-O-Al), in accordance with the Al-avoidance principle (Goldsmith and Laves 1955; Kempster et al. 1962; Megaw et al. 1962). However, an albitic component ($NaAlSi_3O_8$) within anorthite creates Si-O-Si bond sequences, and the strain field associated with these defects may stabilize antiphase boundaries. Even in the absence of albitic substitution, small fluctuations in the degree of Al-Si order may exist on a local scale (Salje 1987; Redfern and Salje 1987), generating a bridging O atom with two Si atoms (Si-O-Si) or two Al atoms (Al-O-Al) as neighbors. Because O is underbonded when it bridges two Al atoms, this configuration may be stabilized by a closer approach of the $Ca^{2+}$ cation to the bridging O atom. Steric hindrance to a shortened Ca-O bond is minimized when the framework is expanded, as should occur locally at the c-antiphase boundary. Therefore, it seems likely that the c-APBs provide an energetically favorable environment for defects that involve Al-Si disorder.

TABLE 3. Diffusion data for Na, $^{24}$Na, and $^{22}$Na in alkali feldspar (Freer 1981)

| Mineral | Diffusing species | $D_0$ (m²/s) | $Q$ (kJ/mol) | $T$ range (K) |
|---|---|---|---|---|
| $Ab_{98}$ | $^{24}$Na | $1.22 \times 10^{-7}$ | 149 | 1123–1213 |
| $Ab_{98}$ | Na | $6 \times 10^{-10}$ | 96 | 1123–1213 |
| $Ab_{98}$ | $^{22}$Na | — | — | 868 |
| $Or_{94}$ | Na | — | — | 1123 |
| $Or_{100}$ | Na | — | — | 1123 |
| $Or_{86}$ | Na | $3 \times 10^{-5}$ | 213.2 | 1018–1324 |
| Perthite | $^{22}$Na | — | — | 823 |

*Note*: $D = 8 \times 10^{-7}$ m²/s for $Ab_{98}$ at 868 K, and $5 \times 10^{-15}$, $2 \times 10^{-14}$, and $(0.1–2.1) \times 10^{-15}$ m²/s for $Or_{94}$, $Or_{100}$, and perthite, respectively.

The kinetics of Al-Si ordering in anorthite have been intensively studied to unravel the complicated series of structural transformations among intermediate plagioclase feldspars (Laves and Goldsmith 1955; John and Müller 1988; Carpenter et al. 1990; Carpenter 1991a, 1991b; Phillips et al. 1992). These investigations all suggest that Al-Si diffusion is extremely sluggish under the conditions of our in situ heating experiments. For instance, TEM work by John and Müller (1988) demonstrated that b-APDs, which reflect Al-Si order, form from anorthite glasses heated to 1300 °C but not 1000 °C. Müller and Wenk (1973) originally suggested that Al-Si disordering is responsible for changes in the average size of c-APDs in anorthite heated to temperatures >1200 °C, and we propose that Al-Si order is the cause of the exact retention of c-APD configurations when anorthite is annealed at <1200 °C.

As noted by Carpenter (personal communication), a relationship between the state of Al-Si order and the $P\bar{1}$-$I\bar{1}$ transition is supported by Landau-based thermodynamic treatments of the phase transitions of anorthite (Salje 1987; Redfern and Salje 1987; Redfern et al. 1988; Redfern and Salje 1992; Redfern 1992). These studies demonstrate that the $P\bar{1}$-$I\bar{1}$ transition (defined by the order parameter $Q_o$) is strongly coupled to the Al-Si ordering process (described by the order parameter $Q_{od}$ of the $C\bar{1}$-$I\bar{1}$ transition) by a strain-induced coupling mechanism.

TABLE 4. Diffusion distances of Na impurities in anorthite

| Annealing $T$ (°C) | $t$ (s) | Diffusion distance (μm) |
|---|---|---|
| 941 | 600 | 5.33 |
| 941 | 600 | 5.16 |
| 591 | 2000 | 0.40 |
| 841 | 600 | 1.73 |
| 841 | 600 | 3.46 |
| 941 | 600 | 3.47 |
| 541 | 600 | 0.81* |

*Note:* Distances calculated by using the corresponding data in Table 3.
* Assuming $D = 1.1 \times 10^{-15}$ m²/s.

The c-APB can be expressed as an interface across which $Q_o$ reverses its sign, and the local structure at the boundary itself is of $I\bar{1}$ symmetry ($Q_o = 0$) (Carpenter 1994). Because $Q_o$ and $Q_{od}$ are coupled, variations in $Q_o$ through a c-APB are favored in regions in which $Q_{od}$ fluctuates because of local Al-Si disorder. The sluggish nature of Al-Si interdiffusion allows no change in the state of $Q_{od}$, so that local Al-Si disorder is responsible for the memory behavior observed.

Although Al-Si disorder appears to be the primary factor that controls the positions of c-APBs, the cage cations may play a secondary role. The substitution of $Na^+$ for $Ca^{2+}$ is accompanied by the replacement of Al by Si for charge compensation, and some authors have suggested that diffusion of Na and Ca through the plagioclase structure is coupled with an Si-Al exchange, resulting in "CaAl-NaSi interdiffusion" (Grove et al. 1984). Electrostatic calculations by Smyth and Smith (1969) suggest that this coupling is energetically favorable. Because Al-Si interdiffusion presumably is the rate-limiting factor in this process, the kinetics of CaAl-NaSi interdiffusion are more similar to those of Al-Si diffusion than to those of Ca-Na diffusion (Grove et al. 1984).

## Acknowledgments

We acknowledge invaluable discussions of anorthite memory behavior with M.A. Carpenter and E.K.H. Salje and constructive reviews of this manuscript by M.A. Carpenter, D.R. Peacor, and G.L. Nord, Jr. We thank P. Dunn and P. Pohwat at the National Museum of Natural History for providing quartz and anorthite specimens, Bin Fu for computer assistance, E.P. Vicenzi for help with microprobe analyses, and A. Navrotsky, T.C. Onstott, and D.R. Veblen for helpful insights and comments. This research was supported by NSF grant EAR-9206031 and EAR-9418031. Electron microscopy was performed at the General Motors Electron Microbeam Facility of the Princeton Materials Institute.

## References cited

Adlhart, W., Frey, F., and Jagodzinski, H. (1980) X-ray and neutron investigations of the $P\bar{1}$-$I\bar{1}$ transition in pure anorthite. Acta Crystallographica, A36, 450–460.

Aslanyan, T.A., Levanyuk, A.P., Vallade, M., and Lajzerowicz, J. (1983) Various possibilities for formation of incommensurate superstructure near the α-β transition in quartz. Journal of Physics C, 16, 6705–6712.

Bachheimer, J.P. (1980) An anomaly in the β phase near the α-β transition of quartz. Journal de Physique-Letters, 41, L559–L561.

Barber, D.J., and Wenk, H.-R. (1991) Dauphine twinning in deformed quartzites: Implications of an in situ TEM study of the α-β phase transformation. Physics and Chemistry of Minerals, 17, 492–502.

Brady, J.B. (1995) Diffusion data for silicate minerals, glasses, and liquids. In T.J. Ahrens, Ed., Mineral physics and crystallography: A handbook of physical constant, p. 269–290. American Geophysical Union, Washington, D.C.

Brown, W.L., Hoffman, W., and Laves, F. (1963) Über kontinuierliche und reversible Transformationen des Anorthits ($CaAl_2Si_2O_8$) zwischen 25 und 350 °C. Naturwissenschaften, 50, 221.

Carpenter, M.A. (1978) Nucleation of augite at antiphase boundaries in pigeonite. Physics and Chemistry of Minerals, 2, 237–251.

——— (1988) Thermochemistry of aluminum/silicon ordering in feldspar minerals. In E. Salje, Ed., Physical properties and thermodynamic behavior of minerals, NATO ASI C, 225, p. 265–323. Reidel, Dordrecht.

Carpenter, M.A., Angel, R.J., and Finger, L.W. (1990) Calibration of Al/Si order variations in anorthite. Contributions to Mineralogy and Petrology, 104, 471–480.

Carpenter, M.A. (1991a) Mechanisms and kinetics of Al-Si ordering in anorthite: I. Incommensurate structure and domain coarsening. American Mineralogist, 76, 1110–1119.

——— (1991b) Mechanisms and kinetics of Al-Si ordering in anorthite: II. Energetics and a Ginzburg-Landau rate law. American Mineralogist, 76, 1120–1133.

——— (1994) Evolution and properties of antiphase boundaries in silicate minerals. Phase Transitions, 48, 189–199.

Cohen, A.J. (1985) Amethyst color in quartz, the result of radiation protection involving iron. American Mineralogist, 70, 1180–1185.

Czank, M., Van Landuyt, J., Schulz, H., Laves, F., and Amelinckx, S. (1973) Electron microscopic study of the structural changes as a function of temperature in anorthite. Zeitschrift für Kristallographie, 138, 403–418.

Dolino, G., and Bachheimer, J.P. (1982) Effect of the α-β transition on mechanical properties of quartz. Ferroelectrics, 43, 77–86.

Foit, F.F., Jr., and Peacor, D.R. (1973) The anorthite crystal structure at 410 and 830 °C. American Mineralogist, 58, 665–675.

Freer, R. (1981) Diffusion in silicate minerals and glasses: A data digest and guide to the literature. Contributions to Mineralogy and Petrology, 76, 440–454.

Frondel, C. (1945) Secondary Dauphine twinning in quartz. American Mineralogist, 30, 447–468.

——— (1962) The system of mineralogy (7th edition), vol 3, Silica minerals, 334 p. Wiley, New York.

Ghose, S., Van Tendeloo, G., and Amelinckx, S. (1988) Dynamics of a second-order phase transition: $P\bar{1}$ to $I\bar{1}$ phase transition in anorthite, $CaAl_2Si_2O_8$. Science, 242, 1539–1541.

Ghose, S., McMullan, R.K., and Weber, H.-P. (1993) Neutron diffraction studies of the $P\bar{1}$-$I\bar{1}$ transition in anorthite, $CaAl_2Si_2O_8$, and the crystal structure of the body-centered phase at 514 K. Zeitschrift für Kristallographie, 204, 215–237.

Goldsmith, J.R., and Laves, F. (1955) Cation order in anorthite ($CaAl_2Si_2O_8$) as revealed by gallium and germanium substitutions. Zeitschrift für Kristallographie, 106, 213–226.

Gordon, W.A., Peacor, D.R., Brown, P.E., Essene, E.J., and Allard, L.F. (1981) Exsolution relationships in a clinopyroxene of average composition $Ca_{0.43}Mn_{0.69}Mg_{0.82}Si_2O_6$: X-ray diffraction and analytical electron microscopy. American Mineralogist, 66, 127–141.

Grove, T.L., Baker, M.B., and Kinzler, R.J. (1984) Coupled CaAl-NaSi diffusion in plagioclase feldspar: Experiments and applications to cooling rate speedometry. Geochimica et Cosmochimica Acta, 48, 2113–2121.

Heaney, P.J., and Veblen, D.R. (1990) A high-temperature study of the low-high leucite phase transition using the transmission electron microscope. American Mineralogist, 75, 464–476.

——— (1991) Observation and kinetic analysis of a memory effect at the α-β quartz transition. American Mineralogist, 76, 1459–1466.

Heaney, P.J. (1994) Structure and chemistry of the low-pressure silica polymorphs. In Mineralogical Society of America Reviews in Mineralogy, 29, 1–40.

Heuer, A.H., and Nord, G.L. (1976) Polymorphic phase transitions in minerals. In H.R. Wenk, Ed., Application of electron microscopy in mineralogy, p. 271–303. Springer-Verlag, Berlin.

Heuer, A.H., Nord, G.L., Lally, J.S., and Christie, J.M. (1976) Origin of the c domains in anorthite. In H.R. Wenk, Ed., Application of electron microscopy in mineralogy, p. 345–353. Springer-Verlag, Berlin.

Inoue, N., Iida, A., and Kohra, K. (1974) X-ray topographic investigation on phase transition in quartz: I. Experimental observations. Journal of the Physical Society of Japan, 37, 742–750.

Jamet, J.P. (1988) Defect-density waves and memory effects in modulated systems. Phase Transitions, 11, 335–371.

John, R.-J., and Müller, W.F. (1988) Experimental studies on the kinetics of order-disorder processes in anorthite, $CaAl_2Si_2O_8$. Neues Jahrbuch für Mineralogie Abhandlungen, 159, 283–295.

Kempster, C.J.E., Megaw, H.D., and Radoslovich, E.W. (1962) The structure of anorthite $CaAl_2Si_2O_8$: I. Structure analysis. Acta Crystallographica, 15, 1005–1017.

Laves, F., and Goldsmith, J.R. (1955) The effect of temperature and com-

position on the Al-Si distribution in anorthite. Zeitschrift für Kristallographie, 106, 227–235.

Laves, F., Czank, M., and Schulz, H. (1970) The temperature dependence of the reflection intensities of anorthite ($CaAl_2Si_2O_8$) and the corresponding formation of domains. Schweizerische Mineralogische und Petrographische Mitteilungen, 50, 519–525.

Liebau, F., and Böhm, H. (1982) On the co-existence of structurally different regions in the low–high-quartz and other displacive phase transformations. Acta Crystallographica, A38, 252–256.

Liu, C.T., Kunsmann, H., Otskuka, K., and Wattig, M., Eds. (1992) Shape-memory materials and phenomena: Fundamental aspects and applications. Materials Research Society Symposium Proceedings, vol. 246, Pittsburgh.

Malov, Y.V., and Sonyushkin, V.E. (1976) Direct electron-microscopic investigation of the α-β transition process in quartz. Soviet Physical Crystallography, 20, 644–645.

Manning, J.R. (1968) Diffusion kinetics for atoms in crystals, 257 p. Van Nostrand, Princeton, New Jersey.

Mazzi, F., Galli, E., aud Gottardi, G. (1976) The crystal structure of tetragonal leucite. American Mineralogist, 61, 108–115.

Megaw, H.D., Kewpster, C.J.E., and Radoslovich, E.W. (1962) The structure of anorthite, $CaAl_2Si_2O_8$: II. Description and discussion. Acta Crystallographica, 15, 1017–1035.

Morimoto, N., and Tokonami, M. (1969) Domain structure of pigeonite and clinoenstatite. American Mineralogist, 54, 725–740.

Müller, W.F., and Wenk, H.R. (1973) Changes in the domain structure of anorthites induced by heating. Neues Jahrbuch für Mineralogie Monatshefte, 17–26.

Müller, W.F. (1988) Antiphasendomänen in anorthit und Ca-reichen plagioklasen. Neues Jahrbuch für Mineralogie Abhandlungen, 158, 139–157.

Nord, G.L., Jr. (1992) Imaging transformation-induced microstructures. In Mineralogical Society of America Reviews in Mineralogy, 27, 453–508.

O'Brien, M.C.M. (1955) The structure of the color centers in smoky quartz. Royal Society of London Proceedings, 231A, 404–441.

Peacor, D.R. (1968) A high-temperature single crystal diffractometer study of leucite, $(K,Na)AlSi_2O_6$. Zeitschrift für Kristallographie, 127, 213–224.

Perkins, J. (1981) Shape memory behavior and thermoelastic martensitic transformations. Materials Science and Engineering, 51, 181–192.

Phillips, B.L., Kirkpatrick, R.J., and Carpenter, M.A. (1992) Investigation of short-range Al,Si order in synthetic anorthite by $^{29}$Si MAS NMR spectroscopy. American Mineralogist, 77, 484–494.

Phillips, B.L., and Kirkpatrick, R.J. (1995) High-temperature $^{29}$Si MAS NMR spectroscopy of anorthite ($CaAl_2Si_2O_8$) and its $P\bar{1}$-$I\bar{1}$ structural phase transition. Physics and Chemistry of Minerals, 22, 268–276.

Redfern, S.A.T. (1992) The effect of Al/Si disorder on the $I\bar{1}$-$P\bar{1}$ co-elastic phase transition in Ca-rich plagioclase. Physics and Chemistry of Minerals, 19, 246–254.

Redfern, S.A.T., and Salje, E. (1987) Thermodynamics of plagioclase: II. Temperature evolution of the spontaneous strain at the $I\bar{1}$-$P\bar{1}$ phase transition in anorthite. Physics and Chemistry of Minerals, 14, 189–195.

——— (1992) Microscopic dynamic and macroscopic thermodynamic character of the $I\bar{1}$-$P\bar{1}$ phase transition in anorthite. Physics and Chemistry of Minerals, 18, 526–533.

Redfern, S.A.T., Graeme-Barber, A., and Salje, E. (1988) Thermodynamics of plagioclase: III. Spontaneous strain at the $I\bar{1}$-$P\bar{1}$ phase transition in Ca-rich plagioclase. Physics and Chemistry of Minerals, 16, 157–163.

Ribbe, P.H., and Colville, A.A. (1968) Orientation of the boundaries of out-of-step domains in anorthite. Mineralogical Magazine, 36, 814–819.

Robie, R.A., Hemingway, B.S., and Fisher, J.S. (1978) Thermodynamic properties of minerals and related substances at 298.15 K and 1 bar ($10^5$ Pascals) pressure and at higher temperatures, 456 p. U.S. Geological Survey, Washington, D.C.

Sadanaga, R., and Ozawa, T. (1968) Thermal transition of leucite. Mineralogical Journal, 5, 321–333.

Salje, E. (1987) Thermodynamics of plagioclase: I. Theory of the $I\bar{1}$-$P\bar{1}$ phase transition in anorthite and Ca-rich plagioclase. Physics and Chemistry of Minerals, 14, 181–188.

Smith, J.V. (1974) Feldspar minerals, vol. 1, Crystal structure and physical properties, 627 p. Springer-Verlag, Heidelberg.

Smith, J.V., and Brown, W.L. (1988) Feldspar minerals, vol. 1, Crystal structures, physical, chemical, and microtextural properties (2nd edition), 828 p. Springer-Verlag, Berlin.

Smyth, J.R., and Smith, J.V. (1969) Electrostatic energy for ion clustering in intermediate plagioclase feldspar. Mineralogical Magazine, 37, 181–184.

Sosman, R.B. (1965) The phases of silica, 388 p. Rutgers University Press, New Brunswick.

Staehli, J.L., and Brinkmann, D. (1974) A nuclear magnetic resonance study of the phase transition in anorthite, $CaAl_2Si_2O_8$. Zeitschrift für Kristallographie, 140, 360–373.

Strukov, B.A. (1989) Global hysteresis in ferroelectrics with incommensurate phases. Phase Transitions, 15, 143–179.

Van Goethem, L., Van Landuyt, J., and Amelinckx, S. (1977) The α-β transition in amethyst quartz as studied by electron microscopy and diffraction. Physica Status Solidi (a), 41, 129–137.

Van Tendeloo, G., Van Landuyt, J., and Amelinckx, S. (1976) The α-β phase transition in quartz and $AlPO_4$ as studied by electron microscopy and diffraction. Physica Status Solidi (a), 33, 723–735.

Van Tendeloo, G., Ghose, S., and Amelinckx, S. (1989) A dynamical model for the $P\bar{1}$-$I\bar{1}$ phase transition in anorthite, $CaAl_2Si_2O_8$: I. Evidence from electron microscopy. Physics and Chemistry of Minerals, 16, 311–319.

Walker, M.B. (1983) Theory of domain structures and associated defects in the incommensurate phase of quartz. Physical Review B, 28, 6407–6410.

Warren, W.L., Dimos, D., and Waser, R.M. (1996) Degradation mechanisms in ferroelectric and high-permittivity perovskites. MRS Bulletin, vol. 21, no. 7, 40–45.

Wayman, C.M. (1980) Some applications of shape-memory alloys. Journal of Metals, 32, 129–137.

Wyart, J. (1938) Étude sur la leucite. Bulletin de la Société Francaise de Mineralogie, 61, 228–238.

Young, R.A. (1962) Mechanism of the phase transition in quartz. U.S. Air Force, Office of Scientific Research, Contract No. AF 49(638)–624.

Zarka, A. (1983) Observations on the phase transition in quartz by synchrotron-radiation X-ray topography. Journal of Applied Crystallography, 16, 354–356.

Manuscript received March 28, 1996
Manuscript accepted October 16, 1996